Effect of (Ce, Al) co-doped ZnO thin films on the Schottky diode properties fabricated using the sol-gel spin coating

MAM Ahmed[*a,b], WE Meyer[a], JM Nel[a]

[a]*Department of Physics, University of Pretoria, Private Bag X20, 0028 Hatfield, South Africa*
[b]*Department of Physics, Faculty of Education, University of Khartoum, P.O Box 461, Omdurman, Sudan*

Abstract

In this work, Schottky diodes based on undoped and (Ce, Al) co-doped ZnO thin films have been fabricated using the sol-gel spin coating. The effect of (Ce, Al) co-doped ZnO films on the structural and optical properties has been studied, and the electrical characteristic of the fabricated Schottky diode devices are investigated. X-ray diffraction and field emission scanning electron microscopy are used to study the crystalline structure and surface morphology, respectively. Room temperature Raman spectroscopy showed that the intensity of the dominant E_2 high peak decreased after doping. The photoluminescence studies at room temperature showed that the intensity of the UV and the visible emission peak decreased after doping. UV-vis spectroscopy measurements at room temperature showed a decrease in the optical band gap after doping compared to undoped ZnO thin films. The *I-V* characteristics of fabricated Schottky diodes manifest good device behaviour at higher levels of doping (7.0 at.%) with an ideality factor of 2.40, the barrier height of 0.77 eV and series resistance of 262 Ω. The maximum rectification ratio was found to be nearly 10^5 at 7.0 at.%. Moreover, the electrical properties of the Schottky diode devices analyzed with Cheung-Cheung function revealed that the Schottky diode parameters were higher compared to those obtained from the conventional thermionic emission theory. Furthermore, the free electron carrier concentration for the doped samples was found to be lower compared with undoped ZnO films.

Keywords: ZnO, Sol-gel; Structural properties; Optical properties; Electrical properties;

1. Introduction

Zinc oxide (ZnO) semiconductor is one of the promising materials in many applications for examples: light emitting diodes (LEDs) [1] chemical and gas sensors [2, 3], optical waveguides [4, 5], solar cells [6, 7], Schottky diodes [8, 9, 10], laser diodes [11], UV-photodiodes [12, 13] and UV-light emitters [14, 15]. ZnO has a high direct band gap of 3.37 eV which make it good for photonic applications in the UV and blue spectral range. Its large exciton energy at room temperature (60 meV) allows emission at room temperature or above to occur. Doping ZnO is considered an effective way to alter the physical and chemical properties of this material. Recently, there have been numerous reports on doping ZnO with metals such as Ag [16, 17], Ga [18, 19], Mn [20, 21] and Al [22, 23]. Amongst these, Al doped ZnO thin films have shown excellent properties such as low cost of fabrication, thermal stability and good resistance to damage by hydrogen plasma [24]. Doping ZnO with Al has also been reported to improve the electrical resistivity. Xu *et al.* [25] found a minimum resistivity of 6.2 $\times 10^{-4}\Omega$.cm when ZnO is doped with 1.5 mol.% Al; however, Parag and his co-worker [24] found a resistivity of 4.4 $\times 10^{-3}\Omega$.cm when ZnO is doped with Al (3.0 at.%). Moreover, Al doped ZnO thin films showed good optical properties [26, 27, 28]. Furthermore, Al doping of ZnO has also been used to produce Schottky devices [29, 30]. Karaagac *et al.* [31] reported a good Schottky device of Al doped ZnO thin films on p-type Si substrate with rectification ratio of five orders of magnitude and an ideality factor of 3.28 fabricated using the sol-gel method. They also found that the band gap increased with increasing Al concentrations.

Email address: mustafa.sonbl@gmail.com (MAM Ahmed[*])

Recently, ZnO has also been doped with rare-earth elements (RE) due to their fluorescence efficiency and the availability of the $4f$ electrons which results in good optical and electrical properties [32]. Many researchers have studied the structural, optical and electrical properties of RE doped ZnO [32, 33, 34, 35]. Amongst these REs Ce doped ZnO has recently shown good electrical and optical properties. Yousefi and co-worker [36] found an enhancement of the photoresponsivity when ZnO is doped with Ce. Narayanan *et. al* [37] found a decrease in the electrical resistivity and an enhancement of the photocatalytic efficiency in spray pyrolysis Ce doped ZnO thin films. Recently, Ce doped ZnO nanorods prepared via chemical bath deposition on an indium coated glass substrate showed good Schottky device properties as shown in our previous work [9].

Many techniques have been used to synthesize ZnO thin films, these include spray pyrolysis [37], metalorganic chemical vapour deposition [38], molecular beam epitaxy [39], RF magnetron sputtering [40] and sol-gel spin coating methods [10, 9, 25, 41]. The sol-gel was adapted in this study due to it is simplicity and versatility of the experimental setup, lower temperature crystallization, low cost, large area production and homogeneity of the produced films. The sol-gel was used to spin coat films on glass for optical and structural characterization, and Si-substrates for device fabrication. As mentioned earlier, Ce and Al doping of ZnO showed good optical and electrical characterization properties. We expect that when ZnO is doped with Al and Ce together will have an impact on the structural, optical and electrical properties. To the best of our knowledge, there is no previous reports on Al and Ce co-doping ZnO on the fabrication of Schottky diodes prepared using sol-gel spin coating method. In this study, the structural, optical and electrical properties of Schottky diodes based on undoped ZnO, Al and Ce co-doped ZnO thin films is studied. ZnO films doped with Ce and Al manifest good device properties with low series resistance and low ideality factor compared to undoped ZnO.

2. Experimental details

Undoped and (Ce, Al) co-doped ZnO thin films [$Zn_{1-x-y}Ce_xAl_yO$, (x = 3.0, 5.0 and 7.0 at.% and y = 1 at.%)] were synthesized using sol-gel spin coating method. Zinc acetate dihydrate (Merck, 98%), cerium nitrate hexahydrate (Sigma Aldrich, 99.999%) and aluminum nitrate nonahydrate (Sigma Aldrich, 99.997%) were used as the starting materials. Isopropanol (Merck, 99.95%) and monoethanolamine (MEA) (Merck, 98%) were used as solvent and stabiliser, respectively. ZnO sol-gel solution was prepared by dissolving zinc acetate dihydrate (0.5M) in a mixture of Isopropanol (60 ml) and MEA (1.8 ml). The solution was then stirred at 500 rpm and 60 °C for 1 h until a transparent, clear and homogeneous solution obtained. Solutions of the dopants were prepared by adding Al (1.0 at.%) and varying amounts of Ce (3.0, 5.0 and 7.0 at.%) to ZnO solution following the same procedure for preparing ZnO sol-gel. All solutions were aged at room temperature for one week before use to increase the viscosity. The molar ratio between zinc acetate and MEA was kept at 1.0 throughout all solutions. Before films deposition, the microscope glass substrates were cleaned in an ultrasonic bath using deionised water, acetone, ethanol and isopropanol for 5 min each and finally blown dry with nitrogen gas. Si substrates were cleaned with trichloroethylene, isopropanol, methanol and deionised water sequentially in an ultrasonic bath for 5 min each. Finally, an HF etch was done before evaporating the ohmic contact. Prior to spin coating the aged sol-gels, we again etched the Si substrates with HF to remove any oxide layer on the surface of the Si. All films were spin coated on a glass and Si substrates at 3500 rpm for 30 s, and after each coating substrates were dried in an oven for 5 min at 200 °C. This procedure was repeated several times until the desired thickness was obtained. Before subjecting to characterizations, films were annealed in a tube furnace at 450 °C for 30 minutes in air.

For the fabrication of ohmic and Schottky contacts, AuSb and Pd were used, respectively. 200 nm of AuSb was evaporated resistively onto the back side of the Si (ρ is 1.4 - 1.8 Ω.cm, thickness of 0.38 μm and carrier concentrations of 2.26 $\times 10^{15}$ cm^{-3}) substrates which was then annealed in Ar atmosphere at 375 °C for 10 min. 100 nm thick Pd circular contact, 0.6 mm in diameter was also evaporated resistively on the top of the thin films using a mechanical mask. The contacts were deposited in a vacuum chamber at a deposition rate of 0.1 nm/s and a pressure of 2.5×10^{-6} mbar. A schematic diagram demonstrating the procedure of preparing the sample and fabricating the Schottky diode device is shown in Fig. 1.

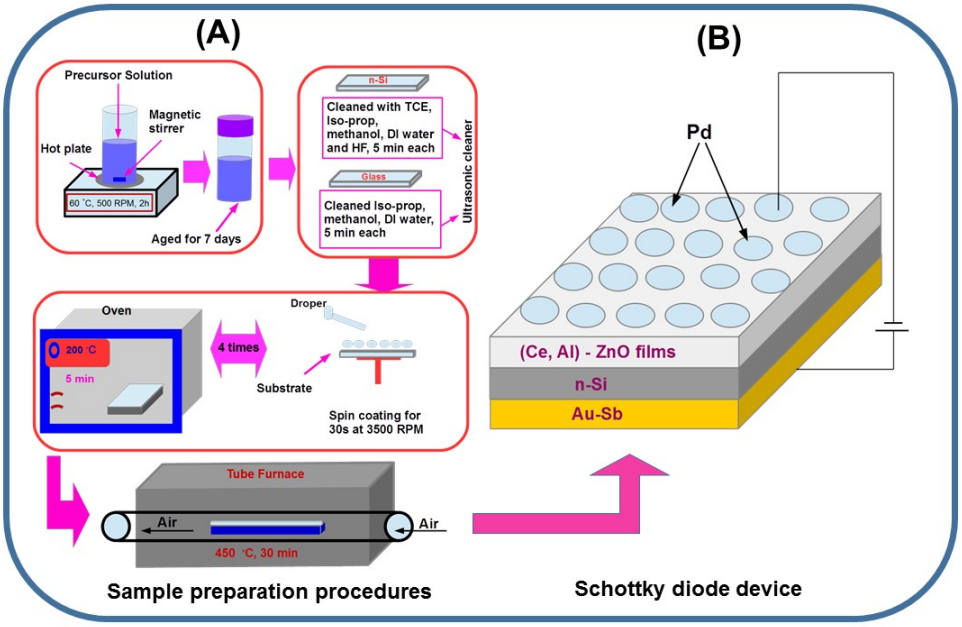

Figure 1: Schematic representation of (A) the procedure for synthesizing the samples and (B) fabricating the Schottky diode.

3. Characterization

Surface morphology and the structure of all films were characterized with Zeiss crossbeam 540 field emission gun scanning electron microscopy (540 FEG-SEM) and a Rigaku SmartLab X-ray diffractometer (λ = 1.54059 nm), respectively. Raman spectroscopy in the range 200 - 1800 nm was measured at room temperature using high-resolution confocal Raman imaging (WITec alpha 300R confocal Raman microscope) with excitation wavelength λ = 532 nm. Room temperature photoluminescence (PL) spectroscopy of all films was studied using 325 nm He-Cd laser in the range 350 - 850 nm. Lambda 950 UV-vis spectrometer was used to measure the optical transmittance at room temperature in the range 200 - 800 nm. Before taking the UV-vis measurements, the background was taken using a pre-cleaned blank optical microscope glass substrate. Finally, the current-voltage (I-V) and capacitance-voltage (C-V) on fabricated Schottky diodes based on undoped ZnO, Ce and Al co-doped ZnO thin films were measured at room temperature using SMU (key sight B2912A) Keithley 230 meter.

4. Results and discussion

4.1. Structural and morphological results

Figure 2 shows the XRD patterns of $Zn_{1-x-y}Ce_xAl_yO$ (x = 0.0, 3.0, 5.0 and 7.0 at.%, y = 1.0 at.%) measured at room temperature. The observed peaks in the XRD pattern are indexed to the wurtzite ZnO structure and cerium dioxide that presents at a higher percentage of Ce doping (7.0 at %) as depicted in Fig. 2. The obtained XRD pattern for undoped ZnO thin films are in good agreement with JCPDS #96−210−7060 with the lattice parameters a = 3.241, c = 5.187 and space group $P6_3mc$. All obtained films are polycrystalline in nature with main peaks being (100), (002) and (101). As can be seen from XRD pattern at lower levels of doping, Ce and Al successfully incorporated into the ZnO lattice and no other peaks related to Ce, Al or other impurities were detected (see Fig. 2 (a), (b) and (c)). The presence of the cerium dioxides peak in the XRD pattern is similar to previously reported [42]. This result indicates that cerium dopant has exceeded the solubility limit. The XRD crystallographic properties of $Zn_{1-x-y}Ce_xAl_yO$ calculated from the XRD data are presented in Table 1. The lattice parameters are calculated as previously described in [9].

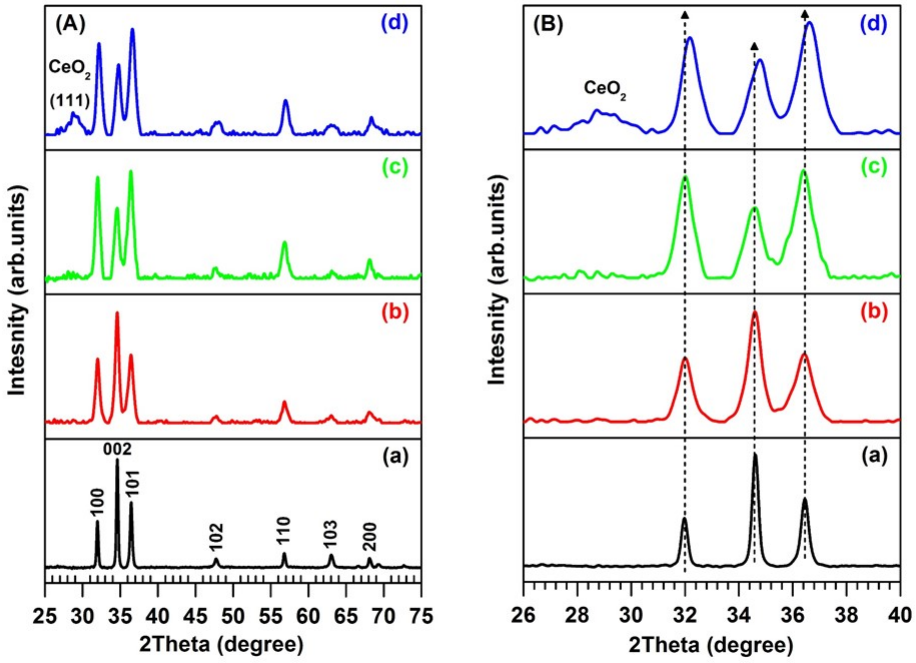

Figure 2: (A) XRD pattern of undoped and (Ce, Al) co-doped ZnO thin films. (B) Is an enlargement of (100), (002) and (101) peaks.

The calculated lattice parameters for undoped ZnO are in good agreement with JCPDS #96 – 210 – 7060. As can be seen from Table 1, the lattice constants decreased with increasing the dopant concentration. This decrease in the lattice parameters could be due to the distortion in ZnO lattice caused by the Ce and Al doping. The lattice constants first increased at Ce and Al concentrations 3.0 at.% and 1.0 at.%, respectively, but decrease for higher Ce concentration (see Table 1). It is also observed from XRD data that, the main peaks (100), (002) and (101) showed a small shift which ensured the incorporation of Ce and Al in ZnO lattice. In the case of (100) and (101) peaks, the shift is toward a higher 2 θ value; however, for the (002) peak the shift is toward lower angle except for the maximum doping which is toward higher 2θ. The small shift indicates that Ce and Al replaced Zn and incorporated into the ZnO lattice. Replacement of Zn^{+2} site by Ce^{+3}/Ce^{+4} and Al^{3+} in lattice may cause crystal defect due to the difference in the ionic radius between the Zn^{+2} (0.74 Å), Ce^{+3}/Ce^{+4} (1.03 Å/0.92 Å) and Al^{+3} (0.53 Å).

It is also noted from Table 1 that, the overall full width at half maximum (FWHM) increased with increasing doping concentration. Moreover, the peaks intensity decreased with increasing the dopants concentrations. The increase in the FWHM and the decrease in the peaks intensity emphasize that the crystal quality of the samples depends on the dopants concentrations [43]. The average crystallite size (D) presented in Table 1, were calculated using Scherrers formula [44] was found to decrease with increasing dopants concentration. This decrease could be attributed to the incorporation of Ce and Al cations into the ZnO crystal lattice which results in a distortion of the lattice due to the higher ionic radius of Ce^{+3}/Ce^{+4} and Al^{+3} together compared to the Zn^{+2} [43, 45, 46, 10].

The growth preferential orientation of all samples was determined from the texture coefficients [43]:

$$TC(hkl) = \frac{I_{(hkl)}/I_0(hkl)}{\frac{1}{N}\sum_n I(hkl)/I_0(hkl)} \quad (1)$$

where $TC(hkl)$ is the texture coefficient, $I_{(hkl)}$ and $I_0(hkl)$ are the measured and the standard relative intensity of plane (hkl), respectively, n is diffraction number of the peaks and N is the reflection number. The texture coefficients are shown in Fig. 3 was calculated from the main three peaks (100), (002) and (101) using Eqn. 1. When $TC(hkl)$ of the

Table 1: Lattice parameters, peak position, FWHM, and the particle size.

$Zn_{1-x-y}Ce_xAl_yO$	Lattice parameter (Å)		2θ	FWHM	D
x, y	a	c	(degree)	(degree)	(nm)
x = 0, y = 0	3.227	5.177			
(100)			31.98	0.278	29.86
(002)			34.61	0.271	30.61
(101)			36.45	0.331	25.06
x = 0.03, y = 0.01	3.225	5.196			
(100)			32.00	0.678	12.24
(002)			34.59	0.624	13.34
(101)			36.48	0.891	9.31
x = 0.05, y = 0.01	3.225	5.188			
(100)			32.00	0.713	9.97
(002)			34.53	0.745	10.38
(101)			36.42	0.704	10.64
x = 0.07, y = 0.01	3.210	5.151			
(100)			32.15	0.664	12.50
(002)			34.79	0.812	10.21
(101)			36.63	0.802	10.34

sample is equal to one, it indicates that the sample is randomly oriented, and the larger $TC(hkl)$ is (i.e. $TC(hkl) > 1$) the higher degree of orientation is along the (hkl) plane. As evidenced in Fig. 3, the preferred orientation for undoped, Ce and Al doped ZnO at 3.0 at.% are along the plane (002). However, the calculated texture coefficients of the rest of the samples were found to be either less than one or almost one.

Figure 4 shows the FESEM images of undoped and (Ce,Al) co-doped ZnO films. SEM shows a uniform film with average particle size ranging from 10.0 - 30.0 nm. The particle size was found to decrease with increasing the dopants concentration. Similar results were also reported for Ce doped ZnO films [36]. It should be mentioned that, the thickness of undoped and (Ce, Al) co-doped ZnO thin films at 0.0, 3.0, 5.0 and 7.0 at.% were found to be 1.3 μm, 900 nm, 1.2 μm and 920 nm, respectively.

4.2. Raman Spectroscopy

Raman scattering measurement is a non-destructive tool that can be used to investigate the vibrational properties of the nanostructured materials and can also give information about phase purity and crystal quality. Fig. 5 shows room temperature Raman spectra of undoped and (Ce, Al) co-doped ZnO thin films measured in the range 200 - 1800 cm^{-1} using laser excitation wavelength 532 nm. At the centre of Brillouin zone (Γ point) the normal vibration mode exists according to the group theory [47, 48]:

$$\Gamma_{Optical} = A_1 + E_1 + 2B_1 + 2E_2 \tag{2}$$

where, A_1, E_1 and E_2 are the first order Raman active modes. B_1 is forbidden, E_1 and A_1 are the polar Raman and infrared active modes, and they split into transverse optical (TO) and longitudinal optical (LO) phonons. According to the Raman selection rules the E_2 and A_1(LO) modes can be observed in unpolarized Raman spectra taken in backscattering geometry [47, 49]. E_2 is nonpolar modes and split into high and low frequency phonon. The Raman spectrum of the samples show several peaks located at 278, 333, 439, 463, 580 and 1100 cm^{-1}. The observed peaks in Raman spectra for undoped, Ce and Al co-doped ZnO thin films up to 5.0 at.% Ce can be assigned to the ZnO wurtzite structure lattice vibration with space group $C^4_{6v}(P6_3mc)$ [50]. Peaks positioned at 333 cm^{-1} and 439 cm^{-1} are assigned to the phonon modes E_2 high - E_2 low and E_2 high, respectively. The peak located at 463 cm^{-1} appeared at higher levels of Ce doping (7.0 at.%) and is assigned to the cerium dioxide [51]. The peak located at 580 cm^{-1} (defects peak) is assigned to the A_1 LO mode [52]. Furthermore, the broad peak between 1100 cm^{-1} and 1200 cm^{-1} is assigned to the multiphonons $2E_1$(LO), $2A_1$ (LO) modes [10, 50, 53].

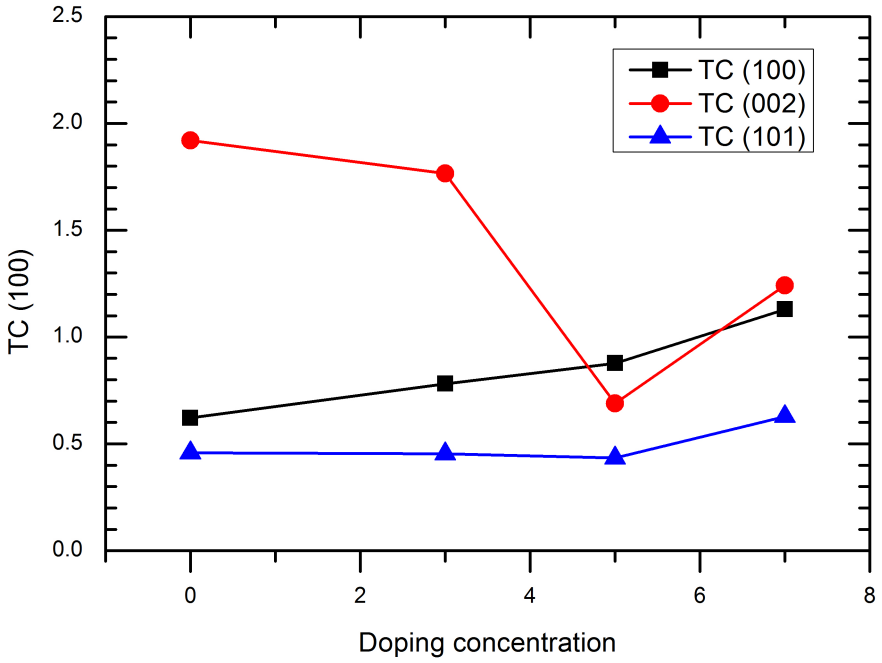

Figure 3: (Color online) TC coefficients of the main diffraction peaks (100), (002) and (101) of undoped and (Ce, Al) co-doped ZnO thin films.

It also observed in Fig. 5 (a) that, the E_2 high peak dominates over the other peaks, which confirmed films of good quality were prepared. The appearance of cerium dioxide peak alongside the ZnO peaks and the decrease of E_2 high intensity in the Raman spectra implies that the quality of the samples is affected by the doping concentration. These results are in good agreement with the XRD presented in the previous section. Moreover, the intensity of the peak located at 580 cm^{-1} increased with increasing dopants concentration, which suggest that the A_1 (LO) peak is influenced by the dopant.

4.3. Photoluminescence

Photoluminescence spectroscopy was carried out to study the luminescence properties of all films. Fig. 6 depicts room temperature PL spectra of undoped, Ce and Al co-doped ZnO thin films with Al concentration fixed at 1.0 at.% and the Ce varying at (3.0, 5.0 and 7.0 at.%). The observed PL spectra consist of two emissions namely, near band edge emission (NBE) and deep level emission (DLE). The NBE can be explained by the free-exciton recombination (i.e. recombination between electron and holes) through exciton-exciton collision process. As shown in Fig. 6 (A), the PL spectra of undoped ZnO sample shows a strong UV emission peak located at 379 nm also known as excitonic emission. Our PL results for undoped ZnO films are similar to previously reported [54]. The appearance of a strong UV emission for undoped ZnO indicates that films with good crystalline quality were prepared. It can also be seen from the PL spectra that the UV emission intensities decreased with increasing dopant concentration and the position of the UV peak showed red-shift compared to undoped ZnO as depicted in Fig. 6 (B). The decrease in the UV emission could be attributed to the effect of doping [55]. The decrease in the UV intensity compared to undoped ZnO sample could also be due to the replacement of the Zn^{+2} with Al^{+3} and Ce^{+3}/Ce^{+4} ions.

A broad visible light (green-orange) emission is observed for all films as shown in Fig. 6 (A) and (B). The undoped ZnO films showed visible light emission in the wavelength range of 450 - 850 nm centered at 640 nm with a weak peak located at 750 nm. The peak at 750 nm has been previously attributed to the vacancies and interstitial of oxygen in

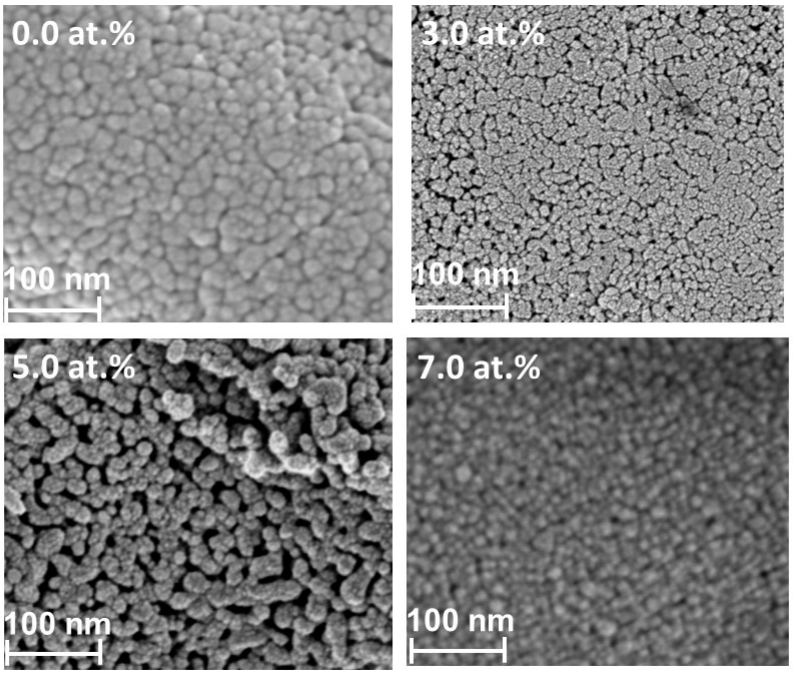

Figure 4: SEM images of undoped and (Ce, Al) co-doped ZnO thin films.

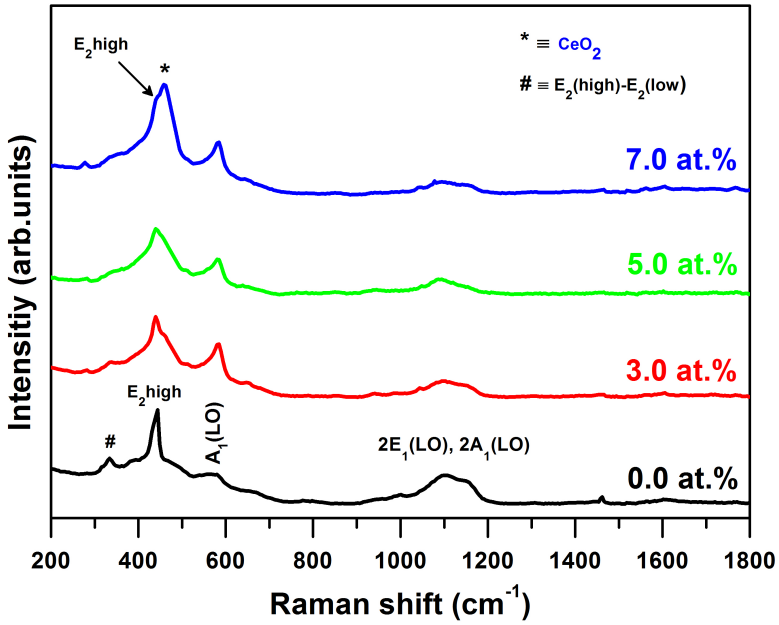

Figure 5: (Color online) Room temperature Raman spectra of undoped and (Ce, Al) co-doped ZnO thin films.

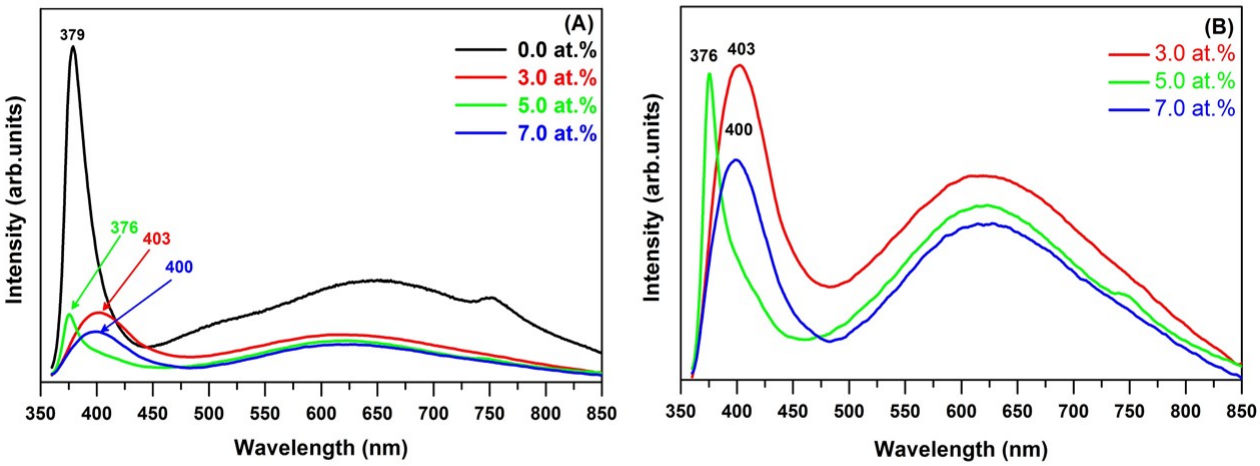

Figure 6: (A) (Color online) PL spectra of undoped and (Ce, Al) co-doped ZnO thin films measured at room temperature. (B) Enlarged scale showing doped samples.

ZnO [54, 56]. As can be seen after doping, the emission peak centre shifted from 640 (red) to 615 (orange emission), and the intensity decreased upon increasing doping (see Fig. 6). Interestingly, the emission peak appeared at 750 nm in undoped ZnO was only observed in the 5.0 at.% Ce films. Generally, green-orange emission has been attributed to surface defects [57], transition between singly ionized oxygen vacancy (V_O^+) and photoexcited hole [58], and transition between electron near to the conduction band and deeply trapped hole (V_O^{++}) [59]. Moreover, the Ce and Al co-doping could also be responsible for the shift and suppression of the green-orange emission. The observed defect emissions in the PL spectra are in good agreement with the defect results seen by Raman spectroscopy discussed in the previous section.

4.4. UV-vis

Figure 7 shows room temperature UV-vis transmittance spectra of undoped and (Ce, Al) co-doped ZnO thin films measured in the range 350 to 800 nm. The transmittance decreased from 56.0 % to 48.0 % at 800 nm for 0.0 and 3.0 at.% Ce, respectively. After that, the transmittance increased to 72.0 % at 5.0 at.% Ce where it shows a maximum, before it drops to 35 % at 7.0 at.% Ce. A similar trend was also reported in our previous work for Ce and Sm doped ZnO [9, 10]. Bronskaya *et al.* [60] reported a transmittance of 75% for trivalent Al (1.5 at.%) and Er (1.0 at.%) co-doping ZnO thin films prepared using the sol-gel spin coating method, which is similar to our spectra for ZnO samples doped at 5.0 at.% in the 200 to 800 nm range. It can be seen from Fig. 7 that, ZnO films doped with 7.0 at.% Ce shows a lower transmittance compared with undoped ZnO, and could be attributed to the higher absorptions in the samples or may be due to the scattering caused by the defect that present in the ZnO due to the doping [61]. It is also observed that all samples do not transmit in the UV light below 300 nm. The optical band gap (E_g) for a direct band gap ZnO semiconductor can be estimated using Tauc's law [62]:

$$(\alpha h\nu)^2 = C(h\nu - E_g) \tag{3}$$

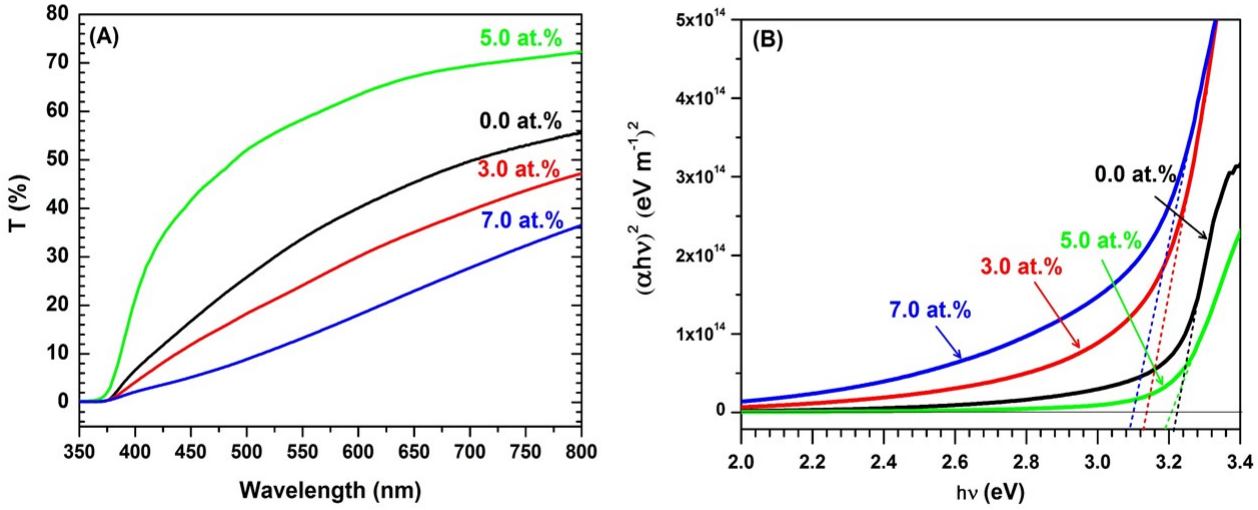

Figure 7: (Color online) (A) UV-vis transmittance spectra and (B) the Tauc plots of undoped and (Ce, Al) co-doped ZnO thin films.

where, $h\nu$ is the phonon energy, C is the proportionality constant and α is the absorption coefficient calculated using equation [62]:

$$\alpha = (\frac{1}{d})\ln(\frac{1}{T}) \tag{4}$$

where, d is the thickness of the film and T is the transmission. The optical band gap energy was extracted from Tauc's plot ($(\alpha h\nu)^2$ vs $h\nu$) by extrapolating linear portion of $(\alpha h\nu)^2$ to zero absorption coefficients ($\alpha = 0$) as shown in Fig. 7 (B). The extracted E_g values for undoped ZnO and (Ce, Al) co-doped ZnO thin films with Al concentration fixed at 1.0 at.% and Ce (3.0, 5.0 and 7.0 at.%) were found to be 3.22, 3.13, 3.20 and 3.10 eV, respectively. We observe that the value of E_g decreased with increasing dopant concentration compared to undoped ZnO. A similar trend was previously observed for Na and K doped ZnO thin films prepared by the sol-gel method [63, 64, 65].

4.5. Current-voltage (I-V) measurements

Figure 8 (A) represent room temperature *I-V* characteristics of the fabricated Pd/n-ZnO/n-Si/AuSb Schottky diodes based on undoped and (Ce, Al) co-doped ZnO thin films with Al concentration fixed at 1.0 at.% and Ce varied as (3.0, 5.0 and 7.0 at.%). As can be seen, all films showed rectification behaviour, and it is positively improved upon doping with Ce and Al. It is also noted that the rectification ratio (I_F/I_R) at +2.0 V increased upon increasing the doping content as depicted in Fig. 8 (A), with the maximum rectification (five orders of magnitude) being obtained with 7.0 at.% Ce (see Fig. 8 (d)). To analyze the *I-V* characteristics of the structure Pd/n-ZnO/n-Si/AuSb Schottky diodes, the thermionic emission theory (neglecting the series resistance) is used [66]:

$$I = I_s\left[\exp\left(\frac{q(V - IR_s)}{k_\beta T}\right) - 1\right] \tag{5}$$

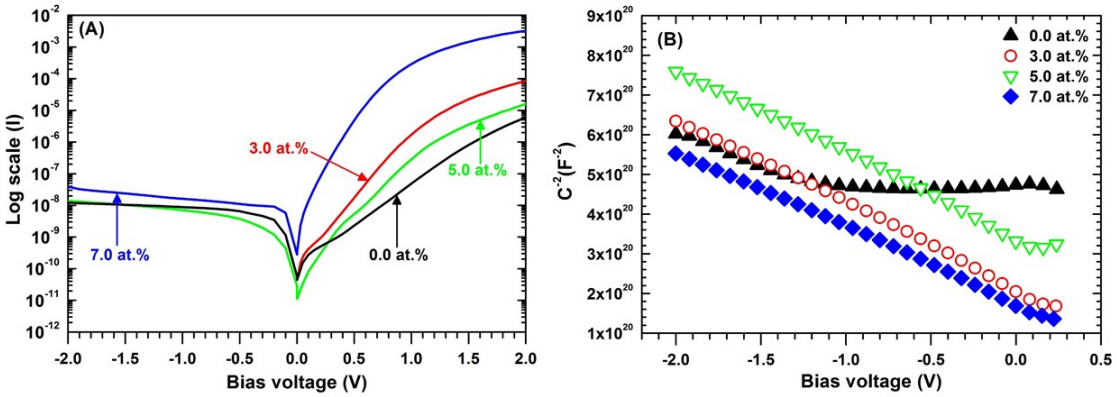

Figure 8: (Color online) (A) and (B) show the *I-V* and *C-V* characteristics of the fabricated Schottky diodes based on undoped and (Ce, Al) co-doped ZnO films, respectively, measured at room temperature.

where, q is the electronic charge, R_s is the series resistance, V is the applied voltage and I_s is the saturation current in the absence of external bias, which it is given by:

$$I_s = AA^*T^2[-q\frac{\Phi_{B_0}}{nk_\beta T}] \tag{6}$$

where, A is the diode contact area ($\approx 2.826 \times 10^{-2}$ cm^2), A^* is the effective Richardson constant (32 Acm^{-2}K^{-2}), Φ_{B_0} represents the zero bias Schottky barrier height defined as $[(kT/q)\ln(AA^*T^2/I_s)]$, k_β is the Boltzmann constant, T is the absolute temperature and n is the diode ideality factor given by $[n = q/k_\beta T[dV/d(lnI)]$, $n = 1$ for an ideal diode]. The obtained n values from the slope of the linear region of *I-V* characteristics presented in Fig. 9. As can be seen, the ideality factor for undoped ZnO is higher than that of the ideal diode, which may be attributed to factors such as series resistance, voltage drop across the metal-semiconductor junction, interface states and interfacial dielectric layers between metal and semiconductor [67, 68], and/or the presence of inhomogeneities in the barrier heights [69, 70]. Our n value for undoped ZnO thin films is in good agreement with previously reported [71]. Upon doping the ZnO, the ideality factor decreased as depicted in Fig. 9, indicating that Ce and Al co-doping affected the electrical properties mentioned above and thus improving the diode quality. Similar results were also reported for Ce doped ZnO nanorods grown on an indium tin oxide substrate [9]. The Φ_{B_0} values obtained from the linear region of *I-V* and *C-V* characteristics at zero applied voltage are also shown in Fig. 9. Φ_{B_0} obtained from *I-V* first increased at Ce level of 3.0 at.% and then decreased with increasing Ce content. It is noted that for all films, the Φ_{B_0} values deviated from the theoretically calculated ~1.0 eV (difference between the Schottky contact work function and the ZnO work function). This deviation could be attributed to the presence of interface states, inhomogeneity of the barrier height at the interface which results in a deviation from the linearity of the *I-V* characteristics [69, 70]. We also observed that the deviation is significantly pronounced in case of undoped ZnO and Ce doped ZnO at 7.0 at.%; however, the deviation is less in case of ZnO samples doped at 3.0 and 5.0 at.%.

Another factor which determined the quality of the diodes is the series resistance. Generally, R_s which is usually modelled with a combination of diode and resistor through which the current I flows. R_s values for films determined from the linear region of the *I-V* characteristics using Ohm's law are also shown in Table 2. In the above mentioned method, the effect of the series resistance on Schottky diodes barrier height and ideality factor was neglected. There-

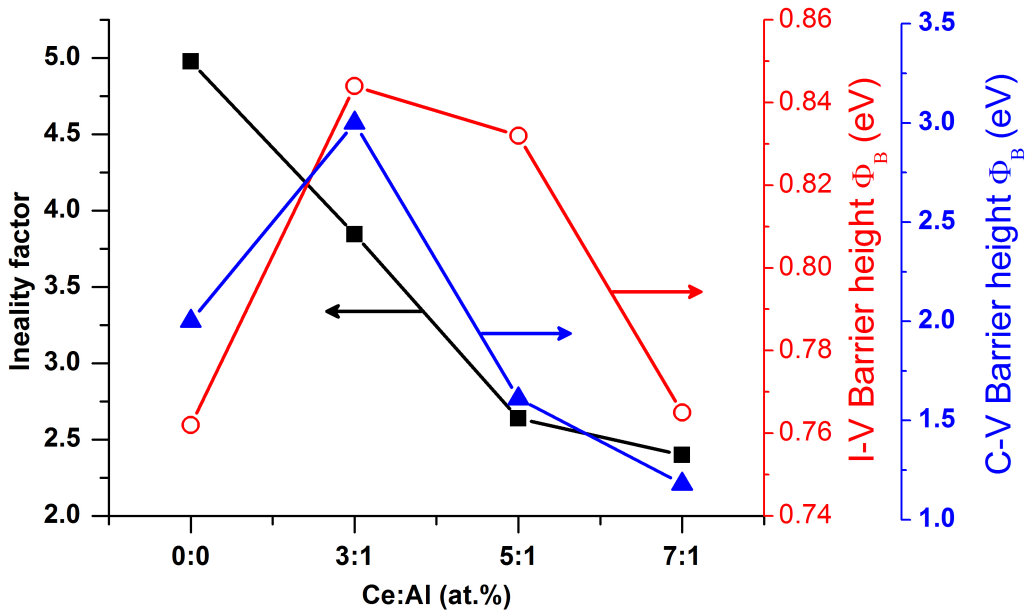

Figure 9: Change in the ideality factor and the SBH obtained from *I-V* and *C-V* characteristics with respect to the doping concentrations.

fore, a more accurate method in determining the Φ_{B_0}, n and R_s is needed. Cheung method [72] is used to extract Φ_{B_0} and n from the forward bias of the *I-V* using the following equations taking into account the effect of R_s:

$$\frac{dV}{d(lnI)} = n\frac{k_\beta T}{q} + IR_s \tag{7}$$

$$H(I) = V - \left(n\frac{k_\beta T}{q}\right) ln\left(\frac{I}{AA^*T^2}\right) \tag{8}$$

$$H(I) = n\Phi_{B_{eff}} + IR_s \tag{9}$$

Figure 10 demonstrate a plot of $dV/d(\ln I)$ and $H(I)$ vs. I. From the linearity of $dV/d(\ln I)$ vs. I, R_s obtained as the slope and the intercept of y-axis represent the $n\frac{K_\beta T}{q}$. By substituting the obtained values of R_s and n in eqn. 8, the value of $H(I)$ is obtained and the plot of $H(I)$ vs. I for all films are shown in Fig. 10 (a) - (d). Now by using a plot of $H(I)$ vs I, the values of R_s and Φ_{Beff} are extracted as the slope and intercept, respectively. The Schottky diode parameters obtained from the thermionic emission and Cheung methods are tabulated in Table 2.

We observe from Table 2 that, the obtained n values using Cheung method is much higher compared to those obtained using ln I vs V, which is attributed to the interface states, the presence of high series resistance, voltage drop across the metal-semiconductor junction and interfacial layer. It is also observed that n values obtained from Cheung method decreased when the R_s is decreased. This confirmed that the value n is affected by the R_s. The estimated values of the Φ_{Beff} using Cheung method for undoped ZnO agrees with the one obtained from ln$I$ vs V; however, a discrepancy is observed more significantly for ZnO doped at 3.0 and 7.0 at.% Ce. This discrepancy could be attributed to the inhomogeneity in the barrier height [73] or non-applicability of the Cheung method to the ZnO doped at 7.0 at.% Ce.

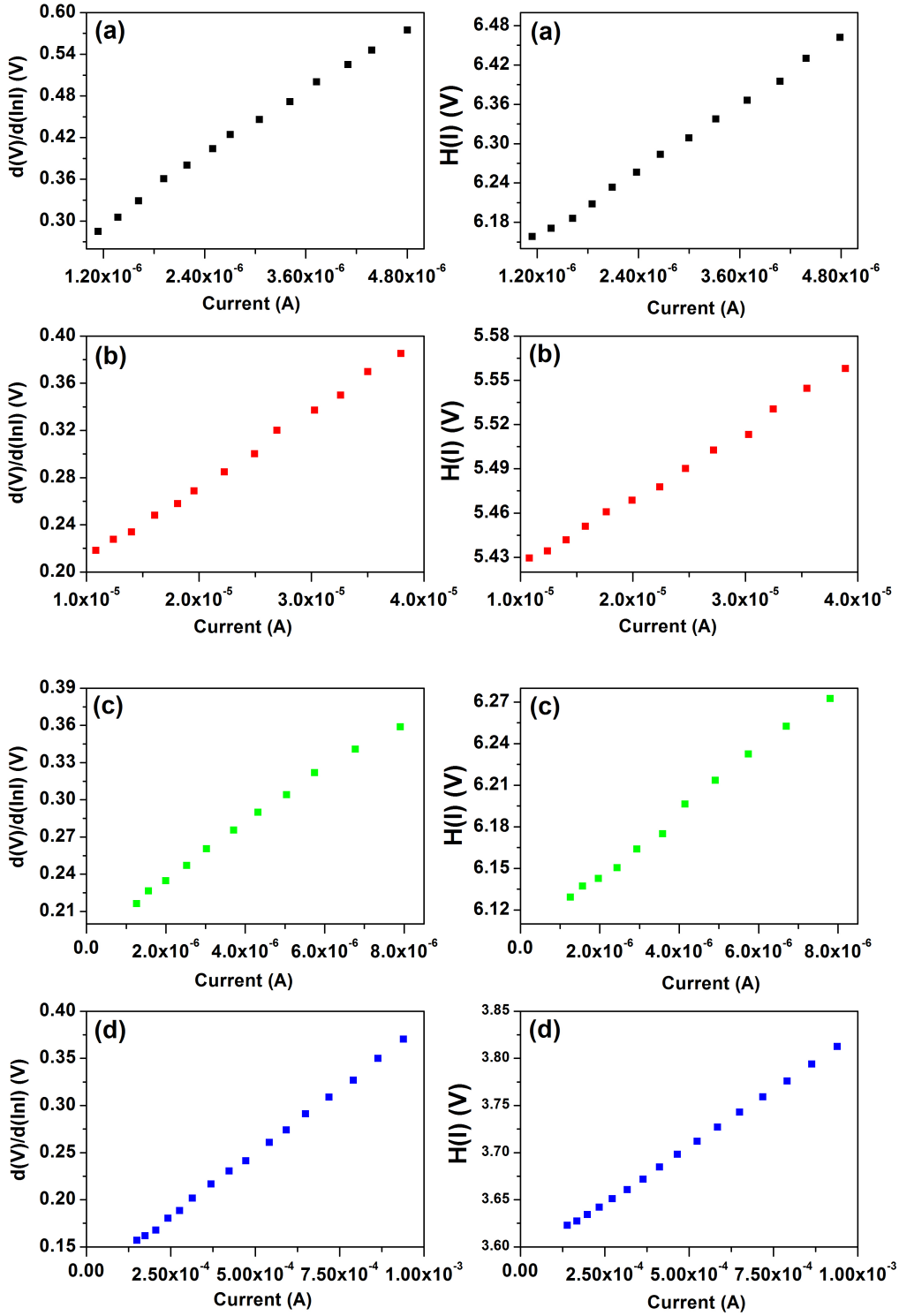

Figure 10: Plot of $d(V)/d(\ln I)$ and $H(I)$ vs I of undoped, and (Ce, Al) co-doped ZnO thin films.

Table 2: Schottky diode parameters evaluated using conventional ln I vs. V and Cheung method and carrier concentration from C-V depth profile for undoped and (Ce, Al) co-doped ZnO thin films.

$Zn_{1-x-y}Ce_xAl_yO$	ln$I$ vs. V			$d(V)/d(\ln I)$			$H(I)$			N_{dcv}
	n	$\Phi_{B_0}(eV)$	$R_s(\Omega)$	n	$\Phi_{B_0}(eV)$	$R_s(\Omega)$	n	$\Phi_{B_{eff}}(eV)$	$R_s(\Omega)$	cm^{-3}
x=0.00,y=0.00	4.97	0.76	42.2k	7.98	-	81.40	-	0.74	81.87k	1.70×10^{17}
x=0.03,y=0.01	3.84	0.84	4.97k	6.98	-	4.29k	-	0.77	5.77k	2.06×10^{16}
x=0.05,y=0.01	2.64	0.83	33.18k	7.58	-	21.92k	-	0.80	289.47	1.15×10^{16}
x=0.07,y=0.01	2.40	0.77	261.97	5.27	-	242.90	-	1.46	257.78	1.04×10^{16}

4.6. Capacitance-voltage (C-V) measurements

Figure 8 (B) shows the C^{-2}-V characteristics of the fabricated Pd/n-ZnO/n-Si/AuSb Schottky diodes based on undoped and (Ce, Al) co-doped ZnO thin films with Al concentration fixed at 1.0 at.% and Ce varied as (3.0, 5.0 and 7.0 at.%) measured at room temperature, and frequency of 1 MHz. The C-V relationship of the Schottky diode is given by:

$$\frac{1}{C^2} = \left(\frac{2}{\epsilon_s \epsilon_0 q N_{dcv} A^2}\right)\left(V_{bi} - V - \frac{kT}{q}\right) \tag{10}$$

where, ϵ_s and ϵ_0 are the permittivity of the semiconductor and free space, respectively, N_{dcv} represent the free electron carrier concentration, and V_{bi} is the built-in voltage (flat band voltage) given by $V_{bi} = V_0 + kT/q$, where V_0 is the x-intercept of $1/c^2$ vs V. The Schottky diode barrier height Φ_B calculated from the C-V characteristics is related to the V_{bi} by the following relation: $\Phi_B = V_{bi} + V_n$ with $V_n = kT/q\ln(N_c/N_d)$ and N_c is the density of states. The V_{bi} values for undoped ZnO and (Ce, Al) at different levels of doping 0.0, 3.0, 5.0 and 7.0 at.% were found to be 1.70, 2.85, 1.35 and 1.18 eV, respectively. The extracted Φ_{B_0} from the linear of C-V characteristics are presented in Fig. 9. It is noted that Φ_{B_0} with increasing the doping concentrations follows the same trend as Φ_{B_0} obtained from I-V characteristics. As has been also observed that the obtained Φ_{B_0} values from the C-V characteristics for the undoped and (Ce, Al) co-doped ZnO thin films were found to larger compared with those obtained from the I-V characteristics, see Fig. 9. This phenomenon has been illustrated as the effect of the thermionic emission on the charge transport, presence of interface states or interfacial layer and also the leakage current [74]. The extracted N_{dcv} values from the depth profile (not shown here) are presented in Table 2. As can be seen in Fig.8 (B) that, the undoped ZnO films showed a kink in the voltage range (-1.0 to 0.20 V). This kink could be attributed to the higher series resistance in the undoped ZnO Schottky device that dominated over the capacitance in the voltage range -1.0 to 0.20 V. After Ce and Al co-doping doing the kink becomes less pronounced except for the ZnO samples doped at 5.0 at.%, which could also be attributed to the series resistance in the Schottky diode device. It should be mentioned that the free electron carrier concentration for the undoped ZnO films was extracted from the linear portion of Fig.8 (B) in the voltage range -2.0 to $\approx$ -1.2 V. Furthermore, the obtained values of N_{dcv} for (Ce, Al) co-doped samples were lower compared to the undoped ZnO films.

5. Conclusion

Pd/ZnO/Sn-Si/AuSb Schottky diodes based on undoped and (Ce, Al) co-doped ZnO thin films were successfully fabricated using low-cost sol-gel spin coating method. The structural, optical and electrical properties were studied in detail. XRD studies revealed that the lattice parameters and particle size decreased with increasing the doping concentration; however, the FWHM increased with increasing doping levels indicating that the dopants incorporated into the ZnO lattice. XRD showed cerium dioxide peak at higher levels of doping emphasising that cerium dopant level at 7.0 at.% was beyond the solubility limit. Raman spectroscopy at room temperature confirmed the wurtzite structure of ZnO by the presence of sharp and intense E_2 high mode. Raman studies also confirmed the presence of the cerium dioxide at maximum levels of doping. PL spectra measured at room temperature showed that the PL spectra consisted of two peaks, UV and broad deep level emission. PL spectra also revealed a decrease in the intensity of both the UV peak and deep level emission after doping, and their position shifted toward higher and lower wavelength, respectively. Maximum transmission obtained ($\sim$ 72%) with 5.0 at.% Ce and 1.0 at.% Al doped ZnO films. The I-V

characteristics measured at room temperature were used to study the electrical properties of the fabricated Schottky diodes. The *I-V* characteristics of all films showed a rectification behaviour with a maximum (nearly five orders of magnitude) obtained with 7.0 at% Ce and 1.0 at.% Al with an ideality factor of 2.40, barrier height of 0.77 eV and series resistance of 262 Ω determined using the conventional thermionic emission method. Moreover, the electrical properties analysed with Cheung method revealed that the Schottky diodes parameters were higher compared with those obtained from the conventional thermionic emission theory. Furthermore, the free electron carrier concentration for the doped samples was found to be lower compared with the undoped ZnO thin films.

Acknowledgment

This work is supported by the South African National Research Foundation (NRF) grant no:91550 and 111744. The opinions, findings and conclusion are those of the authors and the NRF accepts no responsibility whatsoever in this regard. The authors would like to thank Prof. Hendrik Swart, and Prof. Ted Kroon from the department Physics at the University of Free State for XRD and PL measurements.

References

[1] W. Xu, Z. Ye, Y. Zeng, L. Zhu, B. Zhao, L. Jiang, J. Lu, H. He, S. Zhang, ZnO light-emitting diode grown by plasma-assisted metal organic chemical vapor deposition, Appl. Phys. Lett. 88 (17) (2006) 173506.
[2] R. Ahmad, N. Tripathy, M. Ahn, Y. Hahn, Highly stable hydrazine chemical sensor based on vertically-aligned ZnO nanorods grown on electrode, J. Colloid Interface Sci. 494 (2017) 153–158.
[3] A. Umar, M. Rahman, Y. Hahn, Ultra-sensitive hydrazine chemical sensor based on high-aspect-ratio ZnO nanowires, Talanta 77 (4) (2009) 1376–1380.
[4] H. Baek, H. Kwak, S. Song, E. Ha, J. Park, Y. Tchoe, K. Hyun, Y. Park, E. Cheong, G. Yi, ZnO nanotube waveguide arrays on graphene films for local optical excitation on biological cells, Appl. Mater. 5 (4) (2017) 046106.
[5] O. Jamadi, F. Reveret, P. Disseix, F. Medard, J. Leymarie, A. Moreau, D. Solnyshkov, C. Deparis, M. Leroux, E. Cambril, et al., Edge-emitting polariton laser and amplifier based on a ZnO waveguide, Light Sci. Appl. 7 (1) (2018) 82.
[6] M. Patel, H. Kim, J. Kim, J. Yun, S. Kim, E. Choi, H. Park, Excitonic metal oxide heterojunction (NiO/ZnO) solar cells for all-transparent module integration, Sol. Energy Mater. Sol. Cells 170 (2017) 246–253.
[7] X. Dong, D. Chen, J. Zhou, Y. Zheng, X. Tao, High crystallization of a multiple cation perovskite absorber for low-temperature stable ZnO solar cells with high-efficiency of over 20%, Nanoscale. 10 (15) (2018) 7218–7227.
[8] L. Agarwal, B. Singh, S. Tripathi, P. Chakrabarti, Fabrication and characterization of Pd/Cu doped ZnO/Si and Ni/Cu doped ZnO/Si Schottky diodes, Thin Solid Films 612 (2016) 259–266.
[9] M. Ahmed, W. Meyer, J. Nel, Structural, optical and electrical properties of a Schottky diode fabricated on Ce doped ZnO nanorods grown using a two step chemical bath deposition, Mater. Sci. Semicond. Process. 87 (2018) 187–194.
[10] M. Ahmed, S. Mwankemwa, E. Carleschi, B. Doyle, W. Meyer, J. Nel, Effect of Sm doping ZnO nanorods on structural optical and electrical properties of Schottky diodes prepared by chemical bath deposition, Mater. Sci. Semicond. Process. 79 (2018) 53–60.
[11] S. Chu, M. Olmedo, Z. Yang, J. Kong, J. Liu, Electrically pumped ultraviolet ZnO diode lasers on Si, Appl. Phys. Lett. 93 (18) (2008) 181106.
[12] S. Liang, H. Sheng, Y. Liu, Z. Huo, Y. Lu, H. Shen, ZnO Schottky ultraviolet photodetectors, J. Cryst. Growth 225 (2-4) (2001) 110–113.
[13] N. Al-Hardan, A. Jalar, M. Hamid, L. Keng, N. Ahmed, R. Shamsudin, A wide-band UV photodiode based on n-ZnO/p-Si heterojunctions, Sensors Actuat. A Phys. 207 (2014) 61–66.
[14] X. Fang, Y. Bando, U. Gautam, T. Zhai, H. Zeng, X. Xu, M. Liao, D. Golberg, ZnO and ZnS nanostructures: ultraviolet-light emitters, lasers, and sensors, Crit. Rev. Solid State Mater. Sci. 34 (3-4) (2009) 190–223.
[15] F. Qin, C. Xu, Q. Zhu, J. Lu, D. You, W. Xu, Z. Zhu, A. Manohari, F. Chen, Extra green light induced ZnO ultraviolet lasing enhancement assisted by Au surface plasmons, Nanoscale 10 (2) (2018) 623–627.
[16] Y. W. Song, K. Kim, J. P. Ahn, G. E. Jang, S. Y. Lee, Physically processed Ag-doped ZnO nanowires for all-ZnO p–n diodes, Nanotechnol. 20 (27) (2009) 275606.
[17] Y. Li, X. Zhao, W. Fan, Structural, electronic, and optical properties of Ag-doped ZnO nanowires: first principles study, J. Phys. Chem. C 115 (9) (2011) 3552–3557.
[18] M. Yan, H. Zhang, E. Widjaja, R. Chang, Self-assembly of well-aligned gallium-doped zinc oxide nanorods, J. Appl. Phys. 94 (8) (2003) 5240–5246.
[19] H. Wang, S. Baek, J. Song, J. Lee, S. Lim, Microstructural and optical characteristics of solution-grown Ga-doped ZnO nanorod arrays, Nanotechnol. 19 (7) (2008) 075607.
[20] V. Roy, A. Djurišić, H. Liu, X. Zhang, Y. Leung, M. Xie, J. Gao, H. Lui, C. Surya, Magnetic properties of Mn doped ZnO tetrapod structures, Appl. Phys. Lett. 84 (5) (2004) 756–758.
[21] H. Yan, X. Zhong, J. Wang, G. Huang, S. Ding, G. Zhou, Y. Zhou, Cathodoluminescence and room temperature ferromagnetism of Mn-doped ZnO nanorod arrays grown by chemical vapor deposition, Appl. Phys. Lett. 90 (8) (2007) 082503.
[22] Y. Kim, W. Tai, Electrical and optical properties of Al-doped ZnO thin films by sol–gel process, Appl. Surf. Sci. 253 (11) (2007) 4911–4916.
[23] P. VM, S. B. V, K. Balakrishna, K. Naik, Deposition of undoped and Al doped ZnO thin films using RF magnetron sputtering and study of their structural, optical and electrical properties, AIP Conf. Proc. 1832 (1) (2017) 080041.

[24] P. Banerjee, W. Lee, K. Bae, S. Lee, G. Rubloff, Structural, electrical, and optical properties of atomic layer deposition Al-doped ZnO films, J. Appl. Phys. 108 (4) (2010) 043504.
[25] Z. Xu, H. Deng, Y. Li, Q. Guo, Y. Li, Characteristics of Al-doped c-axis orientation ZnO thin films prepared by the sol–gel method, Mater. Res. Bull. 41 (2) (2006) 354–358.
[26] C. Lung, M. Toma, M. Pop, D. Marconi, A. Pop, Characterization of the structural and optical properties of ZnO thin films doped with Ga, Al and (Al^{+1} Ga), J. Alloy Compd. 725 (2017) 1238–1243.
[27] P. Dhamodharan, C. Manoharan, M. Bououdina, R. Venkadachalapathy, S. Ramalingam, Al-doped ZnO thin films grown onto ITO substrates as photoanode in dye sensitized solar cell, Sol. Energy 141 (2017) 127–144.
[28] J. Ghosh, R. Ghosh, P. Giri, Tuning the visible photoluminescence in Al doped ZnO thin film and its application in label-free glucose detection, Sensors Actuat. B Chem. 254 (2018) 681–689.
[29] M. R. Singh, K. Singh, S. Aakanksha, M. Sahni, B. Bhattacharya, P. Gupta, N. Kumar, Deposition and study of AZO heterojunction Schottky diodes at different temperatures, J. Mater. Sci. Mater. Electron. 29 (23) (2018) 20319–20328.
[30] A. Kaya, K. G. Polat, A. S. Mayet, H. Mao, Ş. Altındal, M. S. Islam, Manufacturing and electrical characterization of Al-doped ZnO-coated silicon nanowires, Mater. Sci. Semicond. Process. 75 (2018) 124–129.
[31] H. Karaagac, E. Yengel, M. S. Islam, Physical properties and heterojunction device demonstration of aluminum-doped ZnO thin films synthesized at room ambient via sol–gel method, J. Alloy Compd. 521 (2012) 155–162.
[32] R. Zamiri, A. Lemos, A. Reblo, H. A. Ahangar, J. Ferreira, Effects of rare-earth (Er, La and Yb) doping on morphology and structure properties of ZnO nanostructures prepared by wet chemical method, Ceram.s Int. 40 (1) (2014) 523–529.
[33] J. Sin, S. Lam, K. Lee, A. R. Mohamed, Preparation and photocatalytic properties of visible light-driven samarium-doped ZnO nanorods, Ceram. Int. 39 (5) (2013) 5833–5843.
[34] O. Lupan, T. Pauporte, B. Viana, P. Aschehoug, M. Ahmadi, B. R. Cuenya, Y. Rudzevich, Y. Lin, L. Chow, Eu-doped ZnO nanowire arrays grown by electrodeposition, Appl. Surf. Sci. 282 (2013) 782–788.
[35] M. Balestrieri, G. Ferblantier, S. Colis, G. Schmerber, C. Ulhaq-Bouillet, D. Muller, A. Slaoui, A. Dinia, Structural and optical properties of Yb-doped ZnO films deposited by magnetron reactive sputtering for photon conversion, Sol. Energy Mater. Sol. Cells 117 (2013) 363–371.
[36] M. Yousefi, M. Amiri, R. Azimirad, A. Z. Moshfegh, Enhanced photoelectrochemical activity of Ce doped ZnO nanocomposite thin films under visible light, J. Electroanal Chem. 661 (1) (2011) 106–112.
[37] N. Narayanan, N. Deepak, Realizing luminescent downshifting in ZnO thin films by Ce doping with enhancement of photocatalytic activity, Solid State Sci. 78 (2018) 144–155.
[38] J. Y. Park, D. J. L, S. S. Kim, Size control of ZnO nanorod arrays grown by metalorganic chemical vapour deposition, Nanotechnol. 16 (10) (2005) 2044.
[39] D. C. Look, D. Reynolds, C. Litton, R. Jones, D. Eason, G. Cantwell, Characterization of homoepitaxial p-type ZnO grown by molecular beam epitaxy, Appl. Phys. Lett. 81 (10) (2002) 1830–1832.
[40] R. S. Tondare, B. Shivaraj, H. Narasimhamurthy, M. Krishna, T. Subramanyam, Effect of deposition time on structural, electrical and optical properties of Aluminium doped ZnO thin films by RF magnetron sputtering, Mater. Today Proc. 5 (1) (2018) 2710–2715.
[41] A. Zak, N. Aziz, A. M. Hashim, F. Kordi, XPS and UV–vis studies of Ga-doped zinc oxide nanoparticles synthesized by gelatin based sol-gel approach, Ceram. Int. 42 (12) (2016) 13605–13611.
[42] R. Balboni, R. Lemos, E. Moura, C. Cholant, C. Azevedo, I. Caldeira, A. Gündel, W. Flores, A. Pawlicka, C. Avellaneda, Electrochemical, UV–Vis, and microscopical characteristics of sol–gel CeO_2: V_2 O_5 thin film, J. Mater. Sci.: Mater. Electron. 29 (19) (2018) 16911–16920.
[43] Y. Caglar, Sol–gel derived nanostructure undoped and cobalt doped ZnO: Structural, optical and electrical studies, J. Alloy Compd. 560 (2013) 181–188.
[44] U. Holzwarth, N. Gibson, The scherrer equation versus the'Debye-Scherrer equation', Nat. Nanotechnol. 6 (9) (2011) 534–534.
[45] B. R. Kumar, B. Hymavathi, T. S. Rao, Effect of the ceria dopant on the structural and dielectric properties of ZnO semiconductors, J. Sci. Adv. Mater. Devices 3 433–439.
[46] A. A. Al-Ghamdi, O. A. Al-Hartomy, M. El Okr, A. Nawar, S. El-Gazzar, F. El-Tantawy, F. Yakuphanoglu, Semiconducting properties of Al doped ZnO thin films, Spectrochim. Acta A Mol. Biomol. Spectrosc. 131 (2014) 512–517.
[47] A. Kaschner, U. Haboeck, M. Strassburg, M. Strassburg, G. Kaczmarczyk, A. Hoffmann, C. Thomsen, A. Zeuner, H. Alves, D. Hofmann, et al., Nitrogen-related local vibrational modes in ZnO: N, Appl. Phys. Lett. 80 (11) (2002) 1909–1911.
[48] M. Tzolov, N. Tzenov, D. Dimova-Malinovska, M. Kalitzova, C. Pizzuto, G. Vitali, G. Zollo, I. Ivanov, Vibrational properties and structure of undoped and Al-doped ZnO films deposited by RF magnetron sputtering, Thin Solid Films 379 (1-2) (2000) 28–36.
[49] B. Cheng, Y. Xiao, G. Wu, L. Zhang, The vibrational properties of one-dimensional ZnO: Ce nanostructures, Appl. Phys. Lett. 84 (3) (2004) 416–418.
[50] R. Cuscó, E. Alarcón-Lladó, J. Ibáñez, L. Artús, J. Jiménez, B. Wang, M. J. Callahan, Temperature dependence of Raman scattering in ZnO, Phys. Rev. B 75 (16) (2007) 165202.
[51] S. Wang, W. Wang, J. Zuo, Y. Qian, Study of the Raman spectrum of CeO_2 nanometer thin films, Mater. Chem. Phys. 68 (1-3) (2001) 246–248.
[52] J. Yang, M. Gao, L. Yang, Y. Zhang, J. Lang, D. Wang, Y. Wang, H. Liu, H. Fan, Low-temperature growth and optical properties of Ce-doped ZnO nanorods, Appl. Surf. Sci. 255 (5) (2008) 2646–2650.
[53] C. Du, Z. Gu, M. Lu, J. Wang, S. Zhang, J. Zhao, G. Cheng, H. Heng, Y. Chen, Raman spectroscopy of (Mn, Co)-codoped ZnO films, J. Appl. Phys. 99 (12) (2006) 123515.
[54] V. Kumar, H. Swart, O. Ntwaeaborwa, R. Kroon, J. Terblans, S. Shaat, A. Yousif, M. Duvenhage, Origin of the red emission in zinc oxide nanophosphors, Mater. Lett. 101 (2013) 57–60.
[55] A. Chelouche, T. Touam, M. Tazerout, F. Boudjouan, D. Djouadi, A. Doghmane, Low cerium doping investigation on structural and photoluminescence properties of sol-gel ZnO thin films, J. Lumin. 181 (2017) 448–454.
[56] X. Wang, Z. Li, X. Cao, Z. Wang, Z. Li, Fabrication of a spontaneously bent ZnO nanowire with asymmetrical dots by UV irradiation, RSC Adv. 7 (60) (2017) 38014–38018.

[57] Y. W. Heo, D. P. Norton, S. J. Pearton, Origin of green luminescence in ZnO thin film grown by molecular-beam epitaxy, J. Appl. Phys. 98 (7) (2005) 073502.
[58] A. van Dijken, E. A. Meulenkamp, D. Vanmaekelbergh, A. Meijerink, The kinetics of the radiative and nonradiative processes in nanocrystalline ZnO particles upon photoexcitation, J. Phys. Chem. B 104 (8) (2000) 1715–1723.
[59] J. Ye, S. Gu, F. Qin, S. Zhu, S. Liu, X. Zhou, W. Liu, L. Hu, R. Zhang, Y. Shi, et al., Correlation between green luminescence and morphology evolution of ZnO films, Appl. Phys. A 81 (4) (2005) 759–762.
[60] V. Malyutina-Bronskaya, A. Semchenko, V. Sidsky, V. Fedorov, Properties of ZnO: Er^{3+} films obtained by the sol–gel method, Semicond. 51 (3) (2017) 392–395.
[61] A. El Fakir, M. Sekkati, G. Schmerber, A. Belayachi, Z. Edfouf, M. Regragui, F. Cherkaoui El Moursli, Z. Sekkat, A. Dinia, A. Slaoui, et al., Influence of Rare Earth (Nd and Tb) Co-Doping on ZnO Thin Films Properties, Phys. Status Solidi C 14 (10) (2017) 1700169.
[62] J. Chen, D. Chen, J. He, S. Zhang, Z. Chen, The microstructure, optical, and electrical properties of sol-gel-derived Sc-doped and Al-Sc co-doped ZnO thin films, Appl. Surf. Sci. 255 (23) (2009) 9413–9419.
[63] N. Kamarulzaman, M. F. Kasim, R. Rusdi, Band gap narrowing and widening of ZnO nanostructures and doped materials, Nanoscale Res Lett. 10 (1) (2015) 346.
[64] L. Wang, F. Wu, D. Tian, W. Li, L. Fang, C. Kong, M. Zhou, Effects of Na content on structural and optical properties of Na-doped ZnO thin films prepared by sol–gel method, J. Alloy. Compd. 623 (2015) 367–373.
[65] L. Xu, X. Li, J. Yuan, Effect of K-doping on structural and optical properties of ZnO thin films, Superlattices. Microstruct. 44 (3) (2008) 276–281.
[66] E. Rhoderick, R. Williams, M.-S. Contacts, 2nd edn, Clarendon, Oxford.
[67] L. J. Brillson, Y. Lu, ZnO Schottky barriers and ohmic contacts, J. Appl. Phys. 109 (12) (2011) 8.
[68] N. S. Singh, L. Kumar, A. Kumar, S. Vaisakh, S. D. Singh, K. Sisodiya, S. Srivastava, M. Kansal, S. Rawat, T. A. Singh, et al., Fabrication of zinc oxide/polyaniline (ZnO/PANI) heterojunction and its characterisation at room temperature, Mater. Sci. Semicond. Process. 60 (2017) 29–33.
[69] S. M. Sze, K. K. Ng, Physics of semiconductor devices, John wiley & sons, 2006.
[70] Ş. Aydoğan, K. Çınar, H. Asıl, C. Coşkun, A. Türüt, Electrical characterization of Au/n-ZnO Schottky contacts on n-si, J. Alloy Compd. 476 (1-2) (2009) 913–918.
[71] L. Rajan, C. Periasamy, V. Sahula, Electrical characterization of Au/ZnOthin film Schottky diode on silicon substrate, Perspect. Sci. 8 (2016) 66–68.
[72] S. Cheung, N. Cheung, Extraction of Schottky diode parameters from forward current-voltage characteristics, Appl. Phys. Lett. 49 (2) (1986) 85–87.
[73] M. A. Yıldırım, B. Güzeldir, A. Ateş, M. Sağlam, Temperature dependent current–voltage characteristics of the Zn/ZnO/n-Si/Au–Sb structure with ZnO interface layer grown on n-Si substrate by SILAR method, Microelectron. Eng. 88 (10) (2011) 3075–3079.
[74] A. Srivastava, B. Arora, Effect of annealing on the Richardson constant of Al-GaAs Schottky diodes, Solid-State Electron. 24 (11) (1981) 1049–1052.